Electronic Supplementary Material (ESI) for ChemComm.

Supporting Information

Light-Driven Flagella-Like Motion of Coordination Compound Single Crystals

1. MATERIALS AND METHODS

All the chemicals used were purchased from different commercial resources of high purity and thus were used without any purification. 2tpy was synthesized according to the reported method.[1, 2] NMR spectra were recorded on Bruker 400 MHz. Thermo gravimetric analysis (TGA) was performed under Nitrogen atmosphere with a heating rate of 5°C min^{-1} on a NETZSCH STA 449F3. Leica DM2700M fluorescence microscope attached with high-resolution camera is used to observe the photomechanical motion of single crystals. The acceleration extent of the videos is 1x. The videos were processed using "Clipchamp - video editor" to cut the video as well as to reduce the size of the videos for easy sharing and editorial need. for uploading the files in the manuscript portal.

The Photoluminescence measurements were conducted on HORIBA Jobin Yvon Fluoromax-4 Spectrometer using an excitation wavelength of 370 nm. Time-Resolved Photoluminescence (TRPL) analysis was performed using the HORIBA Scientific DeltaFlexTM and DeltaProTM Fluorescence Lifetime Systems using 407 nm excitation pulses and the software used was EZTime. HRMS data has been obtained using Agilent 6545XT AdvanceBio Q-TOF system. All the UV irradiation reactions were performed under the LUZCHEM UV reactor. In the case of crystalline powders, ground single crystals were packed in between two pyrex glass slides. These grounded single crystals were placed vertically in the LUZCHEM UV reactor to maintain uniform UV exposure.

Details of videos:

Video-1 (Compound 1 Video-1): Light irradiation is from the top (see Fig. 4 of the main manuscript).
Video-2 (Compound 1 Video-2): Light irradiation is from the top.
Video-3 (Compound 1 Video-3): Light irradiation is from the top.
Video-4 (Compound 2 Video-1): Light irradiation is from the top.
Video-5 (Compound 2 Video-2): Light irradiation is from the top.
Video-6 (Compound 2 Crystal bending and elongation): Light irradiation is from the left side (see Fig. 5 of the manuscript).
Video-7 (bending_simulation): Video showing the simulation of bending behaviour (see Fig. 5 of the manuscript).

1. Synthesis and Characterizations

Synthesis of 2tpy: For the preparation of this linker, 4-picoline (5mL) and 2-thiophene carboxaldehyde (7.17mL) in 1: 1.5 molar ratios were taken in a pressure tube. To this, 20 mL of acetic anhydride was added and placed in an oil bath at 140 ºC and 550 – 600 rpm for 48 hrs, followed by workup and washing after 24 hrs. The purification of the compound was done by column chromatography.

Synthesis of [Zn(3,4-DFBA)$_2$(2tpy)$_2$], 1: Yellow needle shaped crystals were obtained by slow evaporation of $Zn(NO_3)_2$ (9.38 mg, 0.033 mmol), 3,4-DFBA (12.51 mg, 0.06 mmol) and 2tpy(6 mg, 0.033 mmol) in methanol after few days and dried at room temperature. ^{1}H NMR (DMSO-d_6, 400 MHz, 298K): δ 8.52 ppm (d, 4H, pyridyl protons of 2tpy), 7.54 ppm (d, 4H, pyridyl protons of 2tpy), 7.32-7.84 ppm (m, 6H, aromatic protons of 2tpy), 7.58-7.84 ppm (m, 6H, 2, 6 DFBA), 7.75 ppm (d, 2H, olefin of 2tpy), 6.93 ppm (d, 2H, olefin of 2tpy).

Synthesis of [Zn(2,6-DFBA)$_2$(2tpy)$_2$].H$_2$O, 2: Yellow needle shaped crystals were obtained by slow evaporation of $Zn(NO_3)_2$ (9.38 mg, 0.033 mmol), 2,6-DFBA (12.51 mg, 0.06 mmol) and 2tpy(6 mg, 0.033 mmol) in methanol after few days and dried at room temperature. ^{1}H NMR (DMSO-d_6, 400 MHz, 298K): δ 8.52 ppm (d, 4H, pyridyl protons of 2tpy), 7.55 ppm (d, 4H, pyridyl protons of 2tpy) 7.00-7.36 ppm (m, 6H, aromatic protons of 2tpy), 7.03 ppm- 7.60 ppm (m, 6H, 2,6-DFBA), 7.78 ppm (d, 2H, olefin of 2tpy), 6.92 ppm (d, 2H, olefin of 2tpy).

X-ray crystallography

Suitable crystals were selected and mounted on a Mitegen loop using Paratone-N oil on a SuperNova, Dual, Cu at home/near, AtlasS2 diffractometer. The crystal was kept at 100(1) K during data collection. Using Olex2[3], the structure was solved with the SHELXT[4] structure solution program using Intrinsic Phasing and refined with the SHELXL[5] refinement package using Least Squares minimization.

Table S1. Cell data for **1** and **2.**

	Compound 1	**Compound 2**
Crystal Data **CCDC Number**	**[Zn(3,4-DFBA)$_2$(2tpy)$_2$]** 2210389	**[Zn(2,6-DFBA)$_2$(2tpy)$_2$].0.5(H$_2$O)** 2210390
Formula	$C_{36}H_{24}F_4N_2O_4S_2Zn$	$C_{36}H_{24}F_4N_2O_4S_2Zn$, 0.5($H_2O$)
Mol. Wt.	754.06	763.07
Crystal system	Monoclinic	Triclinic
Sp. Gr., Z	*P*2/*n*, 2	*P*-1, 4
a, Å	16.0994(3)	7.57920(10)
b, Å	6.08820(10)	21.8875(3)
c, Å	18.3161(3)	22.9265(3)
α, °	90	115.948(2)
β, °	91.838(2)	98.9000(10)
γ, °	90	94.7350(10)
V, Å^3	1794.35(5)	3330.02(9)
D_{calc}**(g/cm^3)**	1.396	1.522
μ **(mm^{-1})**	2.568	2.785
GOF	1.074	1.034
R_1	0.0441	0.0616
wR_2	0.1293	0.1772

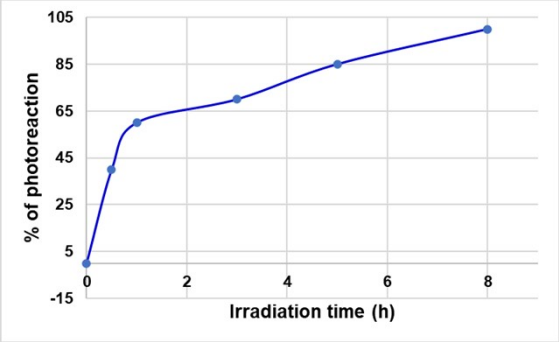

Figure S1. Time dimerization plot of **1**.

HRMS of **1** after the photoreaction has been performed which showed the molecular ion peak at 375.0973 (m/z) and 188.0525 (m/z). Although several attempts were made with different choice of solvents and experimental conditions, metal-complex or polymers couldn't be observed. This might be due to the higher ionizable character of the metal complex.

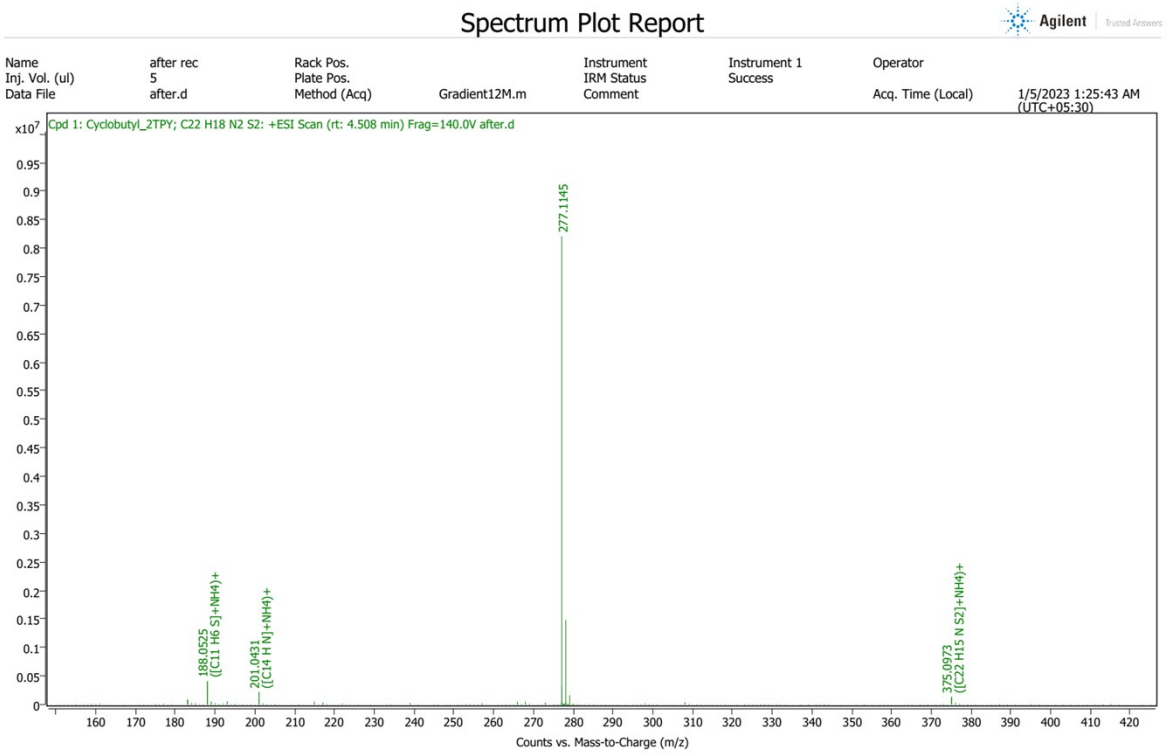

Figure S2. HRMS of **1** after photoreaction.

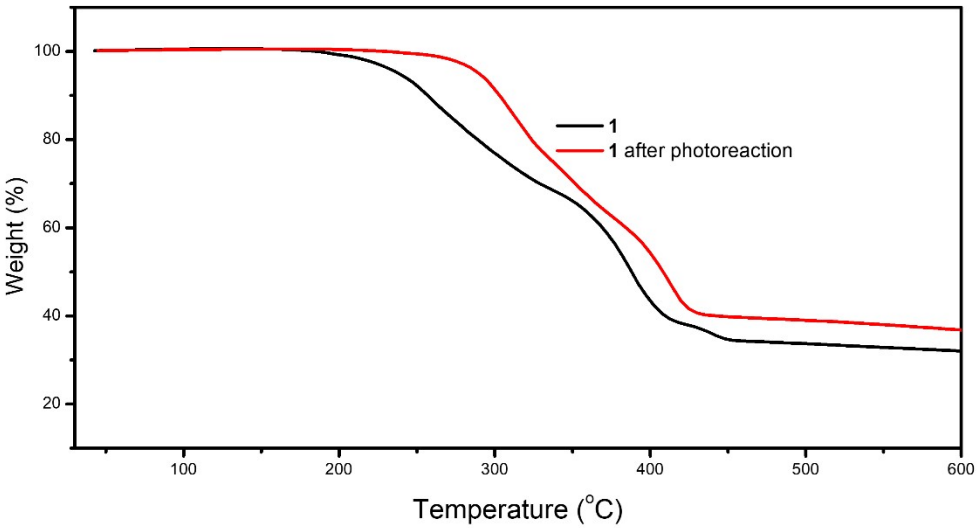

Figure S3. Thermogravimetric analysis of **1** both as synthesized and after the photoreaction.

Non-covalent interactions and details

Compound **1** predominantly exhibits non-covalent interactions, such as π-π interactions between the pyridyl group and thiophene group of neighbouring *head-to-tail* aligned 2tpy ligands. The non-bonded oxygen of 3,4-DFBA has O···H-C=C and O···H-C interaction with the olefinic proton and thiophene proton of 2tpy respectively. There is a C-H···F interaction between the olefinic proton and F-atom of 3,4 DFBA. These interactions altogether assist in aligning the neighbouring group parallel to each other and furnish a possible [2+2] cycloaddition upon UV exposure.

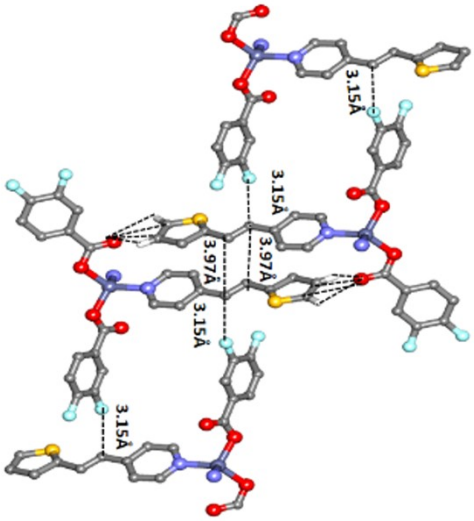

Figure S4. Non-covalent interactions in **1**.

Similar to **1**, compound **2** also exhibits non-covalent interactions such as π-π interactions between the pyridyl group and thiophene group of neighboring *head-to-tail* aligned 2tpy ligands. Other vital interactions like C-H···O from the H-atom of thiophene and O-atom of carboxylate of 2,6-DFBA is present. The non-bonded oxygen of 2,6-DFBA interacts with both

the olefinic proton and thiophene proton of 2tpy. There is a C-H···F interaction between the olefinic proton and F-atom of 2,6-DFBA. These interactions are favorable for a possible [2+2] cycloaddition upon UV exposure.

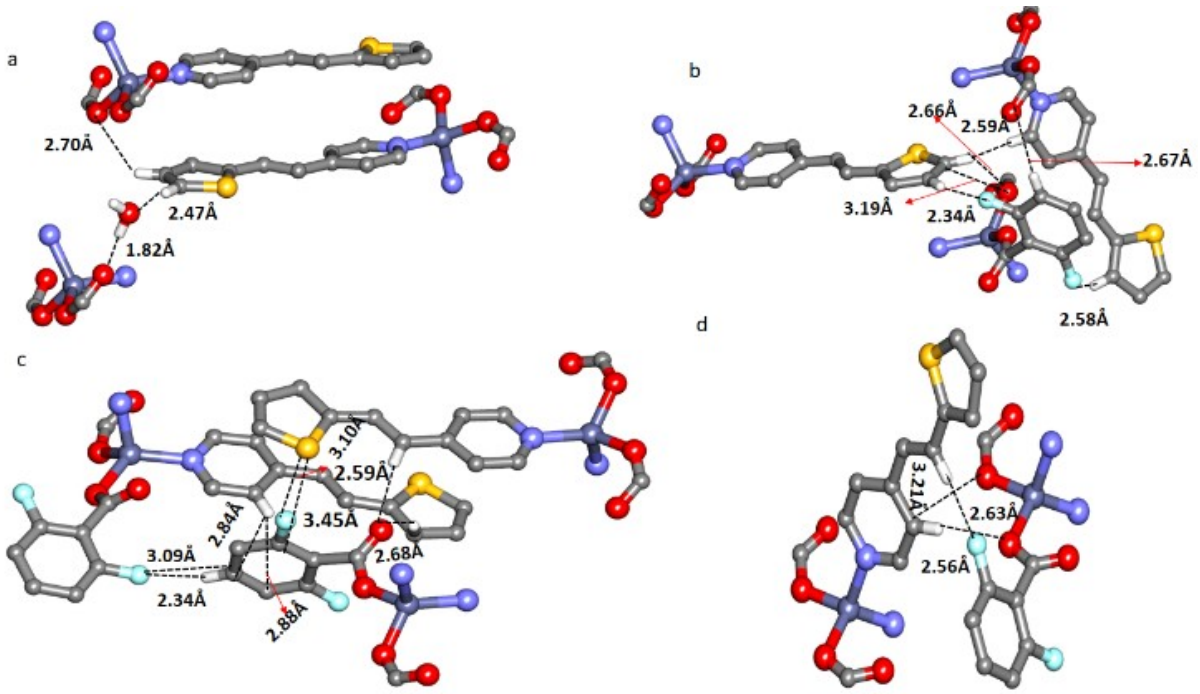

Figure S5. Non-covalent interactions in **2**.

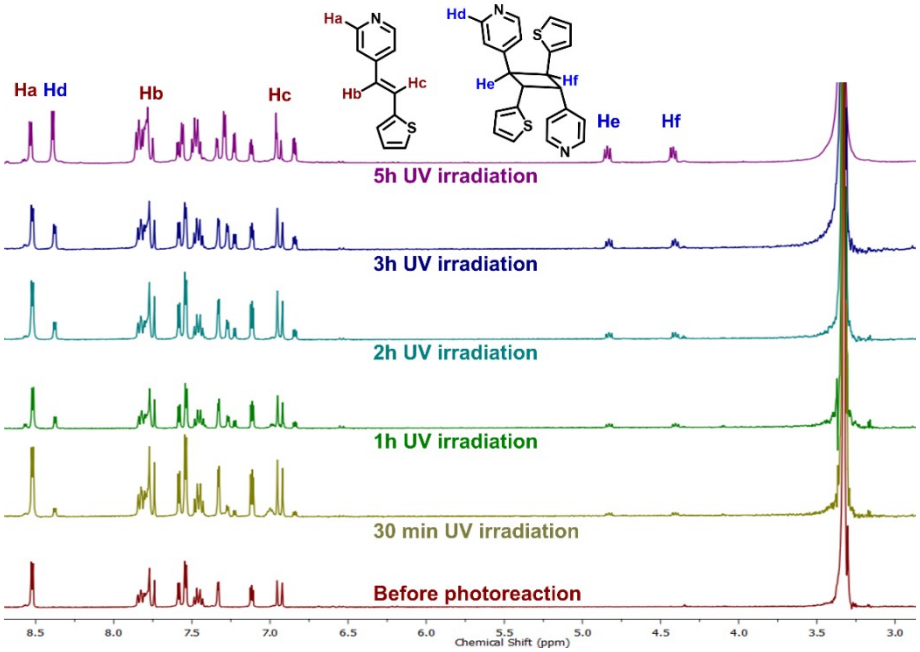

Figure S6. Time dependent ^{1}H NMR plot of **2**.

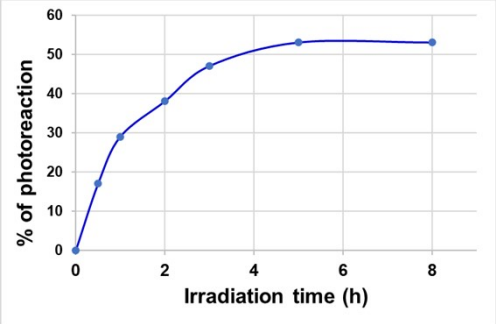

Figure S7. Time dimerization plot of **2**.

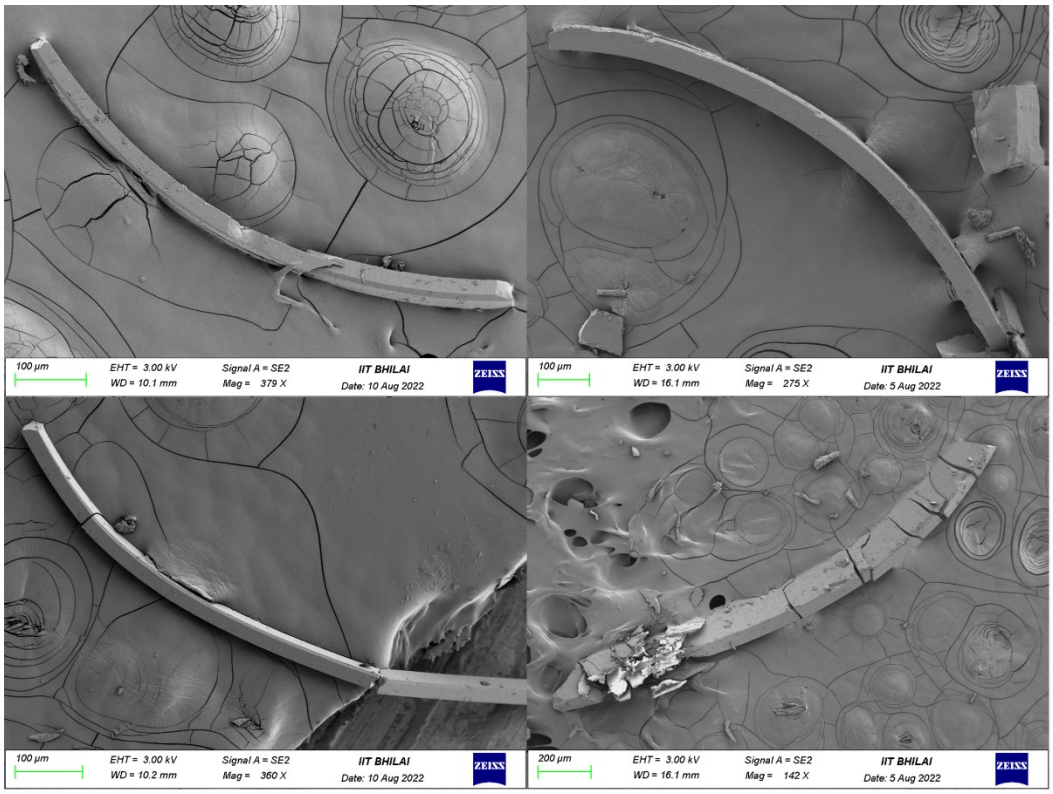

Figure S8. SEM analysis of **1** after bending.

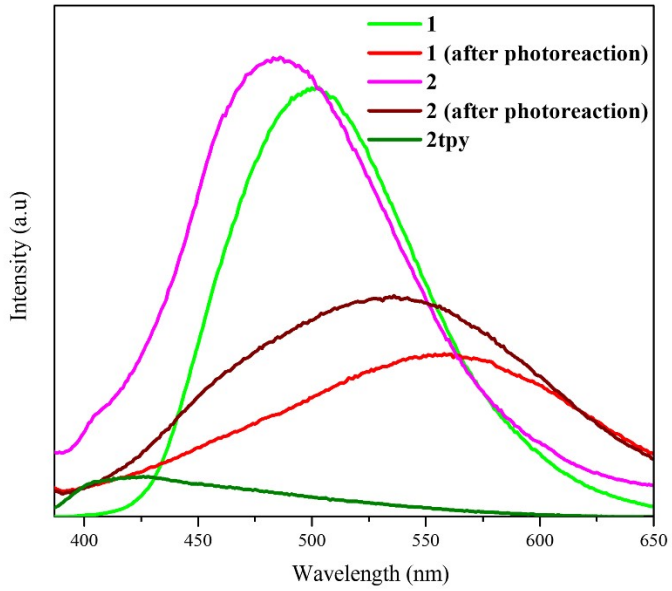

Figure S9. Photoluminescence studies of **1** and **2** both before and after photoreaction.

Table S2. Photoluminescence lifetime of 1 and 2, both before and after the photoreaction

S No	Sample name	T1 (ns)	Std dev	T2 (ns)	Std dev
1	**1** (before photoreaction)	0.1577262	0.006447176	4.215604	0.03556653
2	**1** (after photoreaction)	0.114049	0.0117375	1.69426	0.0992102
3	**2** (before photoreaction)	0.2009214	0.004845733	1.668817	0.0237563
4	**2** (after photoreaction)	0.1168826	0.003896709	1.28512	0.02612099

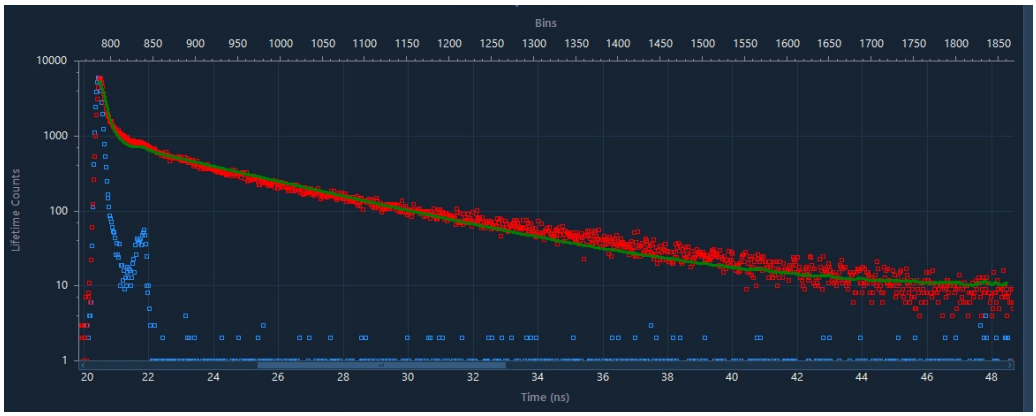

Figure S10. TRPL of **1** before photoreaction (blue dots: instrument response function; red dots: sample measurement).

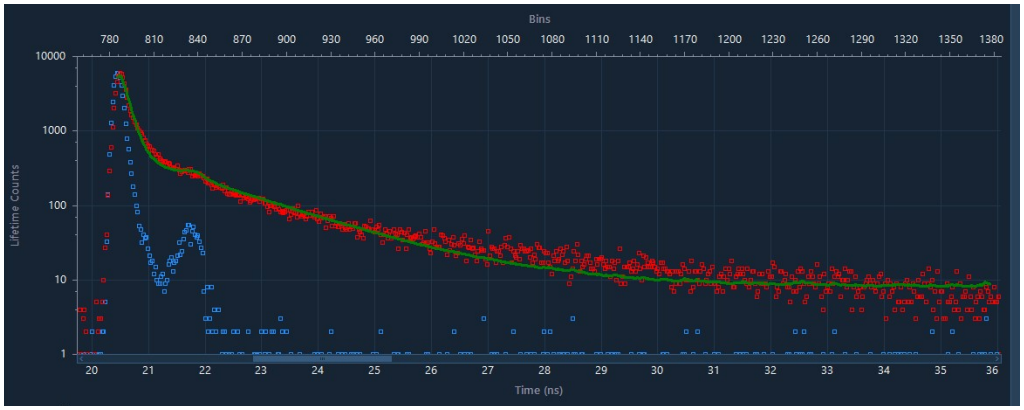

Figure S11. TRPL of **1** after photoreaction (blue dots: instrument response function; red dots: sample measurement).

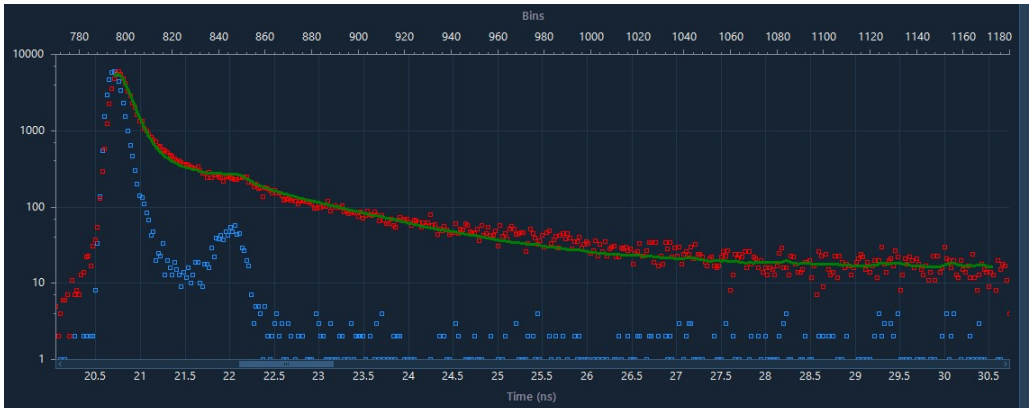

Figure S12. TRPL of **2** before photoreaction (blue dots: instrument response function; red dots: sample measurement).

Figure S13. TRPL of **2** after photoreaction (blue dots: instrument response function; red dots: sample measurement).

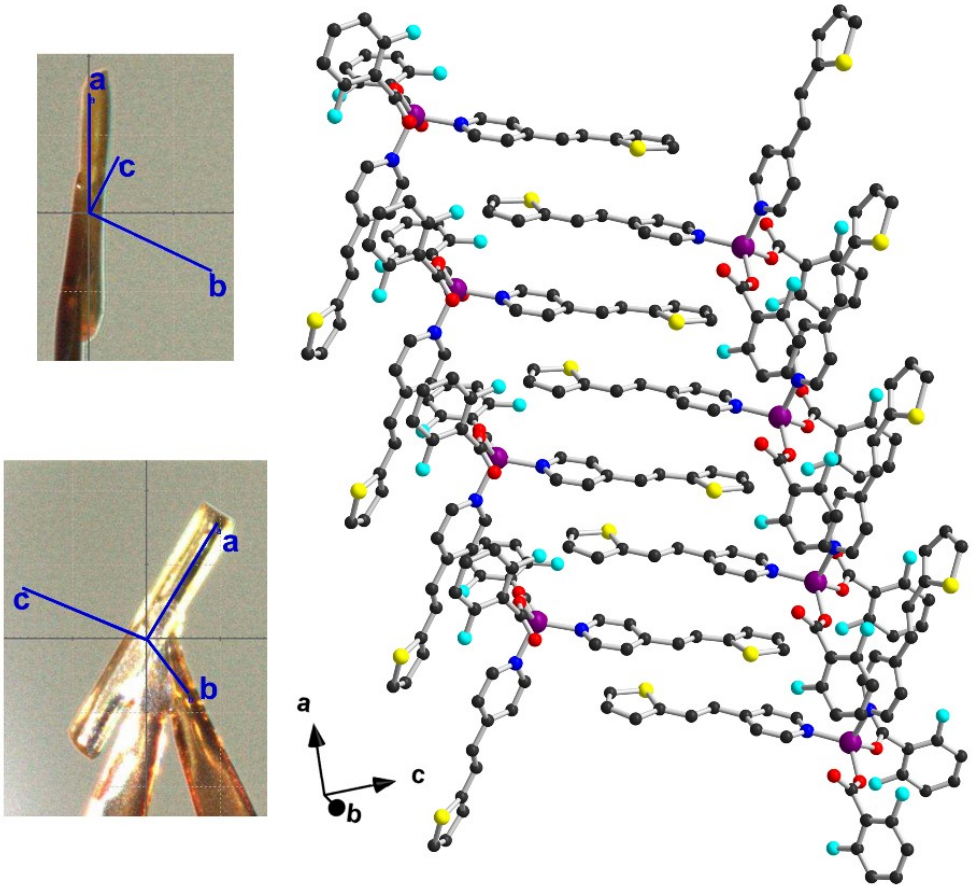

Figure S14. Face indexing of **2** and the arrangement of 2tpy linkers in **2** along *a*-axis.

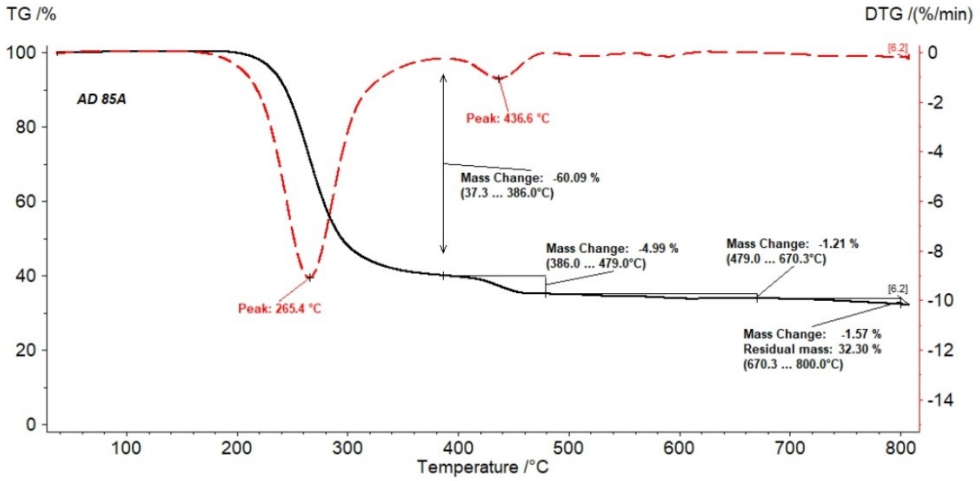

Figure S15. TGA of **2**.

Density analysis

The density of **1** and **2** was measured by floatation method using hexane (density 0.6548 g/ml) and tetrachloroethylene (TCE, density 1.62 g/ml).

Table S3. Percentage of increase in the volume of **1** and **2**.

S.NO	Compound	Density before UV (experimental) g/ml	Density before UV from single crystal XRD data	Density after UV (experimental) g/ml	% of volume increased
1.	1	1.5534	1.524	1.4806	2.931%
2.	2	1.5586	1.425	1.3978	1.94%

Table S4. Average density of **1** and **2** before and after UV.

1 Before UV

Mass (g)	Volume (µL)	Density (g/mL)	Density average (g/mL)
0.1559	100	1.559	
0.1523	100	1.523	
0.1533	100	1.533	1.553
0.1589	100	1.589	
0.1563	100	1.563	

1 After UV

Mass (g)	Volume (µL)	Density(g /mL)	Density average (g/mL)
0.1352	100	1.352	
0.1655	100	1.655	
0.1407	100	1.407	1.4806
0.14789	100	1.4789	
0.15119	100	1.5119	

2 Before UV

Mass (g)	Volume (µL)	Density(g/mL)	Density average (g/mL)
0.15519	100	1.5519	
0.15779	100	1.5779	
0.1539	100	1.539	1.5586
0.15519	100	1.5519	
0.1575	100	1.575	

2 After UV

Mass (g)	Volume (µL)	Density(g /mL)	Density average (g/mL)
0.15519	100	1.5519	
0.15779	100	1.5779	
0.1539	100	1.539	1.3978
0.15519	100	1.5519	
0.1575	100	1.575	

2. Details of numerical simulation model

The model has been designed based on a double metal system exposed to temperature. Photoreaction is simulated as a thermal expansion process. The heat in the simulation is analogous to the light in the experiment. Similarly, the thermal strain (or thermal expansion), the result of heat input in the simulation, is analogous to the photoreaction in the experiment. Further details are discussed as follows:

The crystal is modelled as a plane strain beam of height h. A schematic of the beam is shown in Figure S12. A coupled temperature-displacement problem is solved in a commercial finite element software ABAQUSv2019. Considering the symmetry, only half the beam ($0 \leq x \leq L$) is modeled. The beam is meshed with four-node quadrilateral elements (CPE4T). Displacements of the beam in x and y-directions are constrained at $x = 0$. The exposure of light is modeled by applying a positive temperature difference ΔT at the right surface ($y = 0$) of the beam. All other surfaces ($x = 0$, $x = L$, and $y = h$) are insulated. Material properties used for the simulation do not represent the actual material, and they are chosen to demonstrate the bending.

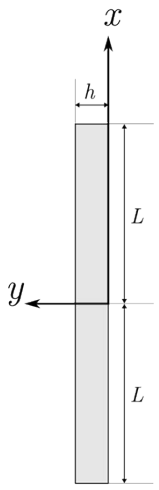

Figure S16. Schematic of the beam.

On the application of temperature at $y = 0$ surface, the temperature in other layers increases because of conduction. Fig. S12 shows the contours of the temperature in the beam. Initially, the varying temperature in different layers results in the non-homogeneous distribution of thermal strain in the beam. This causes the ends of the beam to deflect in the positive y-direction (Fig. S13b). With the heat conducting in other layers of the beam, the non-homogeneity in the thermal strain distribution increases, which deflects the beam further (Fig. S13c). With sufficient time the temperature and the thermal strains distribution start becoming homogeneous, which causes the ends of the beam to bend in reverse direction towards the initial position (Fig. S13d, e, f). Thus, the overall bending behaviour of the crystal has been demonstrated.

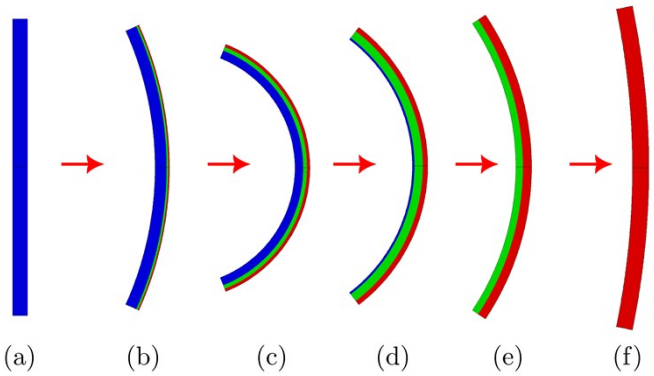

Figure S17. Sequence of beam deformation upon application of temperature. (a) Initially straight beam, (b-c) Bending of beam ends towards left upon application of temperature at *y*=0 surface. Three different colours show zones different of temperature, (d-f) Reverse bending of beam because of more homogeneous distribution of temperature in different layers. Three zones of temperature reduce to two and further to one, displaying the homogeneous distribution of temperature.

3. References

(1) Horwitz, L., Notes - Studies in cis- and trans-Stilbazoles. *J. Org. Chem.* **1956,** *21*, 1039-1041.

(2) Williams, J. L. R.; Adel, R. E.; Carlson, J. M.; Reynolds, G. A.; Borden, D. G.; Ford, J. A., A Comparison of Methods for the Preparation of 2- and 4-Styrylpyridines1. *J. Org. Chem.* **1963,** *28*, 387-390.

(3) Dolomanov, O. V.; Bourhis, L. J.; Gildea, R. J.; Howard, J. A. K.; Puschmann, H., OLEX2: a complete structure solution, refinement and analysis program. *J. Appl. Crystallogr.* **2009,** *42*, 339-341.

(4) Sheldrick, G., SHELXT - Integrated space-group and crystal-structure determination. *Acta Crystallogr. Sect. A.* **2015,** *71*, 3-8.

(5) Sheldrick, G., Crystal structure refinement with SHELXL. *Acta Crystallogr. Sect. C.* **2015,** *71*, 3-8.